HUMAN GENE THERAPY 21:1093–1103 (September 2010)

DOI: 10.1089/hum.2010.040

Magnetic Resonance Imaging-Guided Delivery of Adeno-Associated Virus Type 2 to the Primate Brain for the Treatment of Lysosomal Storage Disorders

E. Aguilar Salegio,[1] A.P. Kells,[1] R.M. Richardson,[1] P. Hadaczek,[1] J. Forsayeth,[1] J. Bringas,[1] S.P. Sardi,[2] M.A. Passini,[2] L.S. Shihabuddin,[2] S.H. Cheng,[2] M.S. Fiandaca,[1] and K.S. Bankiewicz[1]

Abstract

Gene replacement therapy for the neurological deficits caused by lysosomal storage disorders, such as in Niemann-Pick disease type A, will require widespread expression of efficacious levels of acid sphingomyelinase (ASM) in the infant human brain. At present there is no treatment available for this devastating pediatric condition. This is partly because of inherent constraints associated with the efficient delivery of therapeutic agents into the CNS of higher order models. In this study we used an adeno-associated virus type 2 (AAV2) vector encoding human acid sphingomyelinase tagged with a viral hemagglutinin epitope (AAV2-hASM-HA) to transduce highly interconnected CNS regions such as the brainstem and thalamus. On the basis of our data showing global cortical expression of a secreted reporter after thalamic delivery in nonhuman primates (NHPs), we set out to investigate whether such widespread expression could be enhanced after brainstem infusion. To maximize delivery of the therapeutic transgene throughout the CNS, we combined a single brainstem infusion with bilateral thalamic infusions in naive NHPs. We found that enzymatic augmentation in brainstem, thalamic, cortical, as well subcortical areas provided convincing evidence that much of the large NHP brain can be transduced with as few as three injection sites.

Introduction

Lysosomal storage diseases (LSDs) are caused by a variety of recessive gene mutations leading to impaired lysosomal function typically related to the accumulation of metabolites that can interfere with normal cellular function. There are approximately 41 distinct genetic LSDs that range in incidence from about 1 per 57,000 live births (Gaucher disease) to 1 per 4.2 million live births (sialidosis). Niemann-Pick disease is an LSD and can be divided into three types. Type C is caused by mutations in the NPC-1 gene, whereas types A and B are both caused by mutations in acid sphingomyelinase (ASM) that result in hepatosplenomegaly. However, of the two, only type A is associated with a significant neurological deficit, and this difference is most probably due to the different levels of residual enzyme activity in various tissues (Graber *et al.*, 1994). The fact that quite low residual levels of ASM in type B disease prevent the neurological symptoms seen in type A suggests that replacement gene therapy will not require massive overexpression of the ASM transgene. Accumulation of sphingomyelin and cholesterol in neurons is associated with neurological damage. $ASM^{-/-}$ mice develop ataxia due to massive loss of Purkinje cells in the cerebellum (Otterbach and Stoffel, 1995). The exact molecular mechanism by which this occurs is still unclear. However, accumulation of aberrant metabolites of sphingomyelin, such as sphingosylphosphocholine, may cause toxic changes in neurons, such as alterations in transcription patterns and influx of Ca^{2+} (Berger *et al.*, 1995).

Because enzyme replacement therapy is effective only in treating peripheral symptoms (Barton *et al.*, 1991), genetic replacement therapy is a critical avenue to explore for the treatment of the CNS component of the disease. In this respect, Niemann-Pick disease type A (NPD-A) is a template for the development of genetic therapies for the neurological manifestations of other LSDs. Various vectors such as adenoviral (Peltola *et al.*, 1998; Ziegler *et al.*, 1999), lentiviral (Bosch *et al.*, 2000; Kim *et al.*, 2004), and adeno-associated

[1]Department of Neurosurgery, University of California San Francisco, San Francisco, CA 94103.
[2]Genzyme, Framingham, MA 01701.

viral (AAV) vectors have been used in a number of models of LSD (Barranger and Novelli, 2001; Hsich *et al.*, 2002; Watson and Wolfe, 2003). The efficacy studies most relevant to the present work, however, have been those in which $ASM^{-/-}$ mice received intracerebral injections of an AAV vector encoding human ASM. The first study (Passini *et al.*, 2005) showed that treatment of $ASM^{-/-}$ mice with AAV2-hASM corrected the distended lysosomal pathology, and restored normal cholesterol levels in brain (secondary substrate). Moreover, AAV particles underwent axonal transport to distal areas of the brain, despite the fact that projecting neurons were diseased at the time of injection (i.e., even disease-compromised neurons support transport of AAV). Translation of these initial efficacy data from mice into clinical therapy for human infants, however, requires demonstration of effective gene delivery, transport, and expression in the large nonhuman primate (NHP) brain. The present study, therefore, explored vector delivery methods that maximized distribution into key regions of the NHP brain but minimized the number of injections that would be required. We have shown that infusion of AAV2 into NHP thalamus resulted in widespread expression of a secreted transgene (glial cell line-derived neurotrophic factor, GDNF) throughout the cortex (Kells *et al.*, 2009). This focal delivery of vector exploited known thalamocortical projections to drive broad cortical expression in layers III and IV of the cortex. Here we show that AAV2 can also be infused safely into NHP brainstem and bilaterally into thalamus, such that the ASM transgene product can be detected throughout the CNS.

To achieve the safety and accuracy needed for this type of procedure, we performed infusions by magnetic resonance imaging (MRI)-guided, real-time* convective delivery (RCD) (Fiandaca *et al.*, 2009). In this procedure, the coinfusion of a contrast reagent (Gd) with AAV2 particles provides visual feedback to the surgeon performing the infusion as to cannula placement (Yin *et al.*, 2009) and possible untoward reflux or leakage of infusate (Varenika *et al.*, 2008). This study provides a broad gene augmentation strategy for neurological defects in NPD-A that is also likely to be applicable to other LSDs with neurological symptoms.

Materials and Methods

Nonhuman primate subjects

Four NHPs (cynomolgus) were used in this study and were randomized to a 5-week ($n = 2$) or 9-week ($n = 2$) survival group from the time they received their last infusion treatment. No differences in body weight, neurological deficits, or adverse clinical symptoms were observed throughout the study. All procedures were carried out in accordance with the University of California San Francisco (UCSF) Institutional Animal Care and Use Committee. NHPs received either gadoteridol alone (Gd, ProHance; 2 m*M*) or a mixture of AAV2-hASM-HA and Gd. The timeline for all NHP procedures was as follows: baseline MRI (week 0), administration of implants (2 weeks after baseline MRI), Gd-only infusion (2 weeks after implants), Gd plus AAV2-hASM-HA (7 weeks after the Gd-only infusion), and NHP perfusion (5 or 9 weeks after the last AAV infusion).

Adeno-associated viral vector construction

An AAV shuttle plasmid encoding human acidic sphingomyelinase (hASM) (Passini *et al.*, 2005) was modified by inclusion of a sequence at the 3′ end of the ASM cDNA that generated a C-terminal synthetic hemagglutinin epitope derived from viral hemagglutinin in order to facilitate immunodetection of transgene expression in the NHP brain. This shuttle plasmid was then used to manufacture AAV2-hASM-HA (1.0×10^{12} vector genomes [VG]/ml) at the Vector Core at Children's Hospital of Philadelphia (Philadelphia, PA) (Matsushita *et al.*, 1998).

AAV2-hASM-HA infusion

All NHPs underwent a baseline MRI before surgery to visualize anatomical landmarks and to generate stereotactic coordinates of the proposed infusion target sites. NHPs underwent stereotactic placement of the MRI-compatible plastic cannula guide array (12 mm diameter × 14 mm height, containing 27 access holes) for convection-enhanced delivery (CED) into the brainstem and thalamus. Each cannula guide array was secured to the skull with plastic screws and dental acrylic. After placement of the array, animals recovered for at least 2 weeks before initiation of infusion procedures. On the day of infusion, animals were anesthetized with isoflurane (Aerrane; Ohmeda Pharmaceutical Products Division, Liberty Corner, NJ). Each animal's head was then placed in an MRI-compatible stereotactic frame, and a baseline MRI was performed. The selection of cannula tract/access port for each infusion was based on the best trajectory to the targeted region that avoided damage to the lateral ventricles such that the 3-mm step rested in the middle of the targeted region, determined from the MR images (T2-MRI and MP-RAGE [magnetization-prepared rapid gradient-acquisition echo]) acquired in each particular session (see below). Vital signs, such as pulse and partial pressure of oxygen (PO_2), were monitored throughout the procedure. The infusion system consisted of a fused silica reflux-resistant cannula (Krauze *et al.*, 2005; Fiandaca *et al.*, 2008b) connected to a loading line containing the infusate (i.e., Gd only or AAV/Gd), an infusion line filled with mineral oil, and a second infusion line filled with trypan blue solution. A 1-ml syringe, the barrel filled with trypan blue solution, was mounted onto an MRI-compatible infusion pump (Harvard Bioscience, Holliston, MA) that regulated the flow of fluid through the delivery cannula. On the basis of MRI coordinates, the cannula was inserted into the targeted region of the brain through the previously placed cannula guide array. Each infusion cannula was measured to ensure that the distal tip extended 3 mm beyond the cannula step. This created a stepped design that was proximal to the tip of the cannula, maximizing fluid distribution during CED while minimizing reflux along the cannula tract. The infusion cannula was secured, and CED was initiated with the acquisition of MRI data in real time (real-time convective delivery [RCD]). We used the same infusion parameters for every NHP infused throughout the study except that the volume infused ranged from 33 to 199 μl (brainstem, 125–199 μl; thalamus, 33–169 μl). Infusion rates were as follows: 0.1 μl/min was applied when lowering

*In practice, acquisition of the MRI image lags the infusion by 6–12 min.

the cannula to the targeted area (to prevent tissue from entering the tip) and, on reaching the target, increased at 10-min intervals to 0.2, 0.5, 0.8, 1.0, and 2.0 μl/min. Approximately 15 min after infusion, the cannula was withdrawn from the brain. When animals received infusions of Gd alone before AAV2-hASM-HA treatment, the procedure was conducted approximately 4 weeks before the AAV infusions were conducted. Note that all brainstem and thalamic infusions of AAV2-hASM-HA were conducted simultaneously.

Magnetic resonance imaging

NHPs were sedated with a mixture of ketamine (Ketaset, 7 mg/kg, intramuscular) and xylazine (Rompun, 3 mg/kg, intramuscular). After sedation, each animal was placed in a MRI-compatible stereotactic frame. The ear-bar and eye-bar measurements were recorded, and an intravenous line was established. MRI data were then obtained, after which animals were allowed to recover under close observation until able to right themselves in their home cages. MR images for CED infusions delivering Gd alone (total of four) were acquired on a 1.5-T MAGNETOM Avanto (Siemens, Munich, Germany). Three-dimensional (3D) MP-RAGE images were obtained with repetition time (TR) = 2110 msec, echo time (TE) = 3.6 msec, and a flip angle of 15°, number of excitations (NEX) = 1 (repeated three times), matrix = 240×240, field of view (FOV) = 240×240×240 mm, and slice thickness = 1 mm. These parameters resulted in a 1-mm^3 voxel volume. The scanning time was approximately 9 min.

MR images for CED infusions delivering AAV2-hASM-HA/Gd (total of 12) were acquired on a 1.5-T Signa LX scanner (GE Medical Systems, Waukesha, WI) with a 5-inch surface coil on the subject's head, parallel to the floor. SPGR (spoiled gradient recalled) images were T1-weighted and obtained with a spoiled GRASS (gradient recalled acquisition in steady state) sequence, a TR = 2170 msec, a TE = 3.8 msec, and a flip angle of 15°, NEX = 4, matrix = 256×192, FOV = 16 cm×12 cm, and slice thickness = 1 mm. These parameters resulted in a 0.391-mm^3 voxel volume. Scanning time was approximately 11 min.

Tissue processing

NHPs were transcardially perfused with PBS followed by 4% paraformaldehyde (PFA) in PBS. Their brains were harvested and sliced coronally into 6-mm blocks that were postfixed in 4% PFA–PBS and cryoprotected in 30% (w/v) sucrose. A sliding microtome (HM 450; Thermo Scientific, Waltham, MA) was used to cut blocks into 40-μm-thick serial sections that were then processed for histology.

Immunoperoxidase staining

A monoclonal antibody against the hemagglutinin (HA) tag (mouse anti-HA, diluted 1:10,000, clone 16B12; Covance, Princeton, NJ) or ASM (mouse anti-ASM-biotinylated, diluted 1:100; Genzyme, Framingham, MA) was used to detect expression of the human transgene. Briefly, sections were washed with PBS (three times, 5 min each) and were quenched for endogenous peroxidase activity in 1% H_2O_2 in PBS (20 min), and then washed again in PBS as described previously. Sections were blocked for 30 min in Background Sniper (BS966G; Biocare Medical, Concord, CA) and incubated overnight with the HA and/or ASM primary antibody or with anti-biotin-M antibody (mouse, diluted 1:200, MB-9100; Vector Laboratories, Burlingame, CA) in Da Vinci green diluent (PD900; Biocare Medical). The next day, after washing sections in PBS, sections were incubated in MACH 2 mouse HRP polymer (MHRP520; Biocare Medical) for 1 hr, washed in PBS, and developed with 3,3′-diaminobenzidine (DAB) for 6 min (DAB peroxidase substrate kit, SK-4100; Vector Laboratories). DAB-processed sections were washed in PBS, mounted on frosted slides, and counterstained with cresyl violet.

Immunofluorescence staining

Brain sections were immunostained with anti-HA (mouse monoclonal, diluted 1:200; Covance) and either anti-Iba1 (rabbit polyclonal, diluted 1:100, Biocare Medical) or anti-NeuN (mouse, monoclonal, diluted 1:500; Millipore). Alternatively, anti-HA was used in combination with anti-S100 protein (rabbit polyclonal, diluted 1:100; Biocare Medical). Sections were washed with PBS containing 0.1% Tween 20 (PBST; three times for 5 min each), endogenous peroxidase activity was quenched in 1% H_2O_2 in 50% ethanol (30 min), and the sections were washed again in PBST as described previously. Sections were blocked for 60 min in 20% normal horse serum (NHS; Jackson ImmunoResearch, West Grove, PA) and incubated for at least 24 hr at 4°C with each of the primary antibody cocktails in Da Vinci green diluent (PD900; Biocare Medical). After incubation with primary antibodies, sections were washed in PBST, incubated with a cocktail of secondary antibodies (fluorescein isothiocyanate [FITC]-conjugated anti-mouse [diluted 1:200] and tetramethylrhodamine isothiocyanate [TRITC]-conjugated anti-rabbit [diluted 1:200]; Jackson ImmunoResearch) in PBST for 1 hr at room temperature, washed in PBST, and wet-mounted on frosted slides. These sections were coverslipped with a 4′,6-diamidino-2-phenylindole (DAPI)-containing hard-set medium.

Ratio of volume of distribution to volume infused

The volume of distribution (V_d) for each brainstem and thalamic infusion was measured with OsiriX software for the analysis of DICOM images (version 3.6). Briefly, regions of interest (ROIs), defined as the areas of visualized Gd signal on each DICOM, were manually delineated with the ROI tool. Ratios were calculated by taking the volume of the resulting 3D reconstruction of the combined infusate (either Gd only or AAV-hASM-HA/Gd) distribution (V_d) and dividing it by the volume infused (V_i). To compare V_d:V_i ratios for repeated infusions, V_d was measured on DICOM series at equivalent V_i. Note that MRI sequences necessary to quantify tissue concentration as a means to calculate V_d were not acquired. However, the sensitivity of this Gd detection, based on the available images, was sufficient to calculate accurate ROIs manually.

Area of HA immunostaining transferred to MR images

The transference of HA-positive areas was conducted first by scanning (Epson 1660 photo scanner at 300 dpi) all histology-processed slides counterstained with cresyl violet. Bright-field microscopy sections were used to delineate manually the extent and boundary of immunoreactivity per infused region. The resulting outlines were then copied to a

transparency paper, individually matched to the corresponding baseline MR images, and drawn with the Osirix ROI tool. In one instance (NHP1260), MR imaging showed good tracer distribution in the right thalamus, but no transgene expression was detected by immunohistochemistry. It is not clear why this thalamic infusion did not transduce any neurons, but we suspect it might be due to vector aggregation during the procedure (Wright *et al.*, 2003). Nevertheless, in the absence of transgene expression, no analysis was possible and results from the specific thalamic infusion were not included in the study.

Percentage of HA-positive neuronal transduction

In adjacent serial sections (thickness, 40 μm), immunostaining for neuronal marker (anti-NeuN) or HA tag (anti-HA) was performed, and randomized $\times 20$ magnification images ($698 \times 522\,\mu$m) were taken per targeted region (two images per infusion site) across all NHPs ($n = 4$). In these images, neuronal cell bodies stained for NeuN and HA were manually counted, and their number was tabulated and analyzed collectively per region infused (i.e., thalamus and brainstem). Comparison between NeuN- and HA-stained cell bodies was expressed as the percentage of neurons positive for the HA tag per infused region.

Statistical analysis

The distribution of Gd alone and of AAV2-hASM-HA/Gd were compared by Student t test and Pearson's correlation. Results were considered statistically significant when $p < 0.05$.

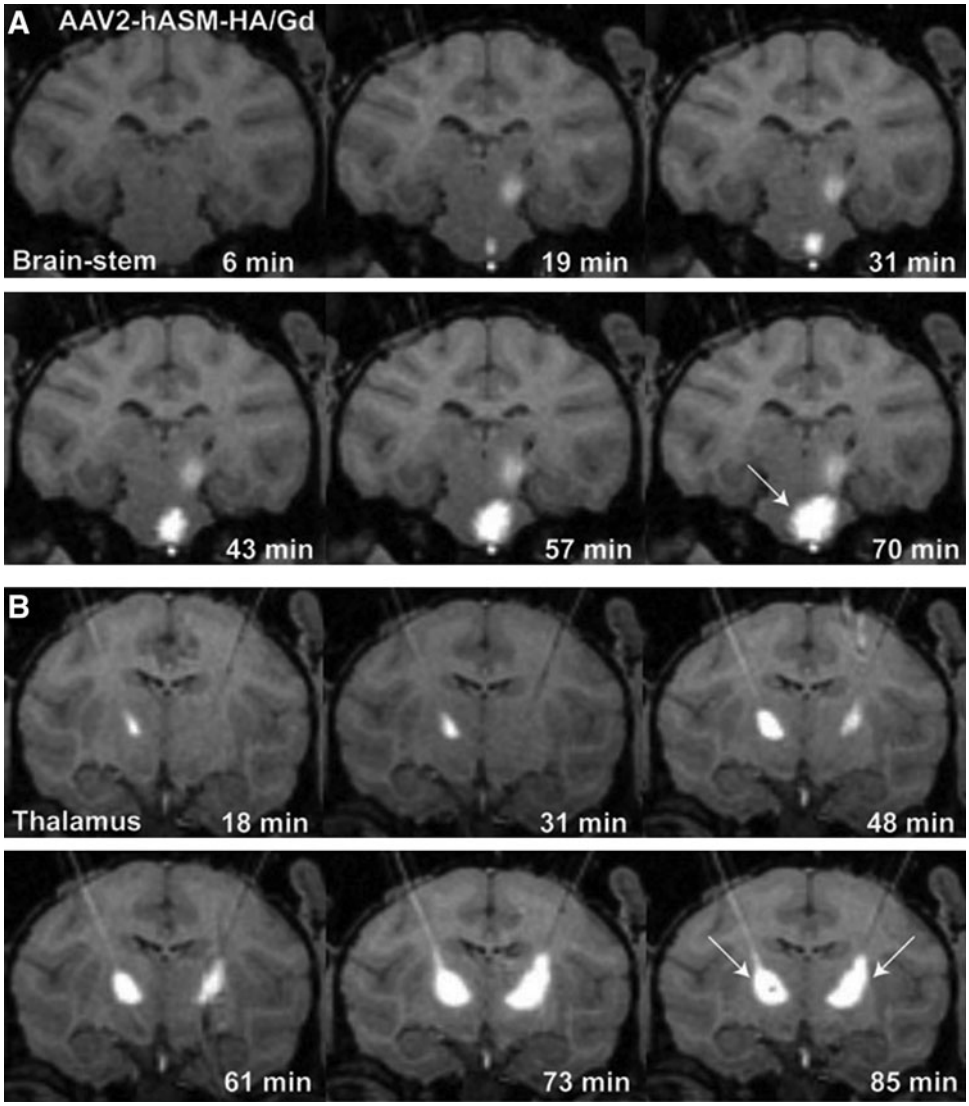

FIG. 1. Intraoperative use of real-time convection-enhanced delivery (CED) in the nonhuman primate (NHP) brainstem and thalamus. Infusion of AAV2-hASM-HA/Gd visualized as a contrast demarcation on MRI indicates cannula tip placement in the targeted region (**A** and **B**; white arrows). Note the increase in infusate size as a function of time as demonstrated in sequential MR image acquisitions. In (**A**), residual contrast signal visible 19 min after initiation of brainstem infusion correlates with diffusion of thalamic signal, completed 30 min before the end of brainstem infusion.

Results

Real-time MR imaging of CED

The outcome of intraoperative MR imaging of cannula placement and monitoring of CED is illustrated in Fig. 1, where the placement of the cannula tip into predetermined brainstem or thalamic structures could be observed with infusion of MRI contrast reagent in all cases (Fig. 1A and B). Unilateral infusions in the brainstem and bilateral infusions in the thalamus were performed simultaneously (Fig. 1A and B, white arrows). Consistent with previous observations from our laboratory, we found radial convection of delivered infusate with no signs of untoward leakage or reflux (Varenika *et al.*, 2008).

Volume infused versus volume of distribution

A direct linear relationship was found between V_d and V_i for brainstem and thalamic infusions ($R^2 = 0.93$; Fig. 2) as previously described for liposomal infusions (Yin *et al.*, 2010). The mean V_d:V_i ratio for brainstem ($n = 6$) was 3.3 ± 0.17 and for thalamus ($n = 10$) it was 3.86 ± 0.25; the ratios were not significantly different from each other ($p = 0.14$). More importantly, we demonstrated that repeated infusions of the MRI tracer into the same anatomical regions resulted in consistent infusate distribution (Fig. 3). We observed similar distribution patterns and V_d:V_i ratios in brainstem and thalamic infusions, with no statistically significance difference between primary and secondary deliveries ($p = 0.96$). Note that, because of the size and volume of the brainstem relative to thalamus, greater volumes were infused into the brainstem region compared with thalamus, with no apparent adverse effects.

AAV transduction and distribution

Robust levels of transduction were achieved in the brainstem and thalamus after targeted infusions into these regions

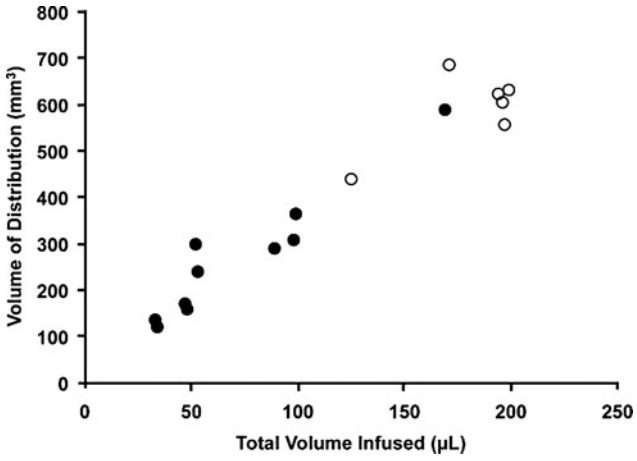

FIG. 2. Coinfusion of AAV2-hASM-HA and gadoteridol (Gd) into the brainstem (open circles) and thalamus (solid circles). Shown are the results of single delivery of various amounts of infusate into the brainstem (open circles, $n = 6$; mean V_i:V_d ratio, 3.3 ± 0.17) and thalamus (solid circles, $n = 10$; mean V_i:V_d ratio, 3.86 ± 0.25). There is a linear relationship between V_d and V_i (overall, $n = 16$, $R^2 = 0.93$), with higher V_i delivered to the brainstem region as compared with the thalamus. No significant difference was found between ratios in these two regions ($p > 0.05$).

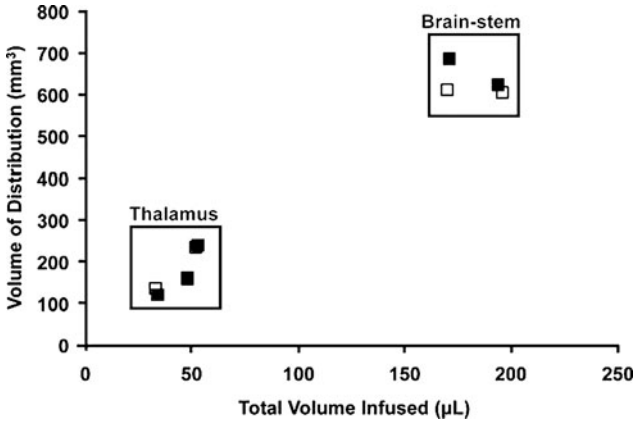

FIG. 3. Comparison of V_d:V_i ratios with repeated brainstem and thalamic infusions. Initial V_d:V_i delivery parameters during Gd-only infusions (solid squares, $n = 5$; mean V_d:V_i ratio, 3.74 ± 0.25; $R^2 = 0.96$) were replicated in later infusions consisting of AAV2-hASM-HA/Gd (open squares, $n = 5$; mean V_d:V_i ratio, 3.72 ± 0.24; $R^2 = 0.98$). Note the consistent distribution patterns in consecutive infusions with or without therapeutic agent (overall, $n = 10$, $R^2 = 0.96$). No significant difference was found between primary and secondary infusions ($p > 0.05$).

(Fig. 4). These images show the transduction of cells resembling neurons or with neuron-like morphology. CED delivery into the thalamus resulted in direct transduction and global distribution of this transgene to cortical regions not directly targeted by the infusion (Table 1). This was indicated by the detection of HA-positive cells dispersed throughout many cortical regions.

Efficiency of transgene expression

Another important factor in the establishment of a successful infusion protocol is the correlation between the distribution of MRI tracer and the resulting area of transgene expression (Fig. 5; Table 2). Counting of neuronal cell bodies, immunostained with the neuronal marker (anti-NeuN) or HA epitope tag (anti-HA), revealed that up to $82 \pm 7.8\%$ of neurons were positive for HA in the brainstem, and $68 \pm 11.3\%$ of neurons were positive in the thalamus. Comparison of the area of transgene expression and that of Gd distribution for brainstem infusions revealed that, in the brainstem, the expression area slightly exceeded the area of MR tracer distribution ($117 \pm 7.2\%$), but in the thalamus the corresponding overlap was only $82 \pm 8.4\%$. Closer examination of transduced regions indicated that the vector specifically transduced neurons (Fig. 6A–C) with no cellular transduction detected in astrocytes (Fig. 6D–F) or microglia (Fig. 6G–I), in agreement with previous demonstrations of the neuronal specificity of AAV2 (Daadi *et al.*, 2006; Cunningham *et al.*, 2008). A modest increase in microglial activation was apparent in directly infused regions (Fig. 6G–I); however, this was confined to the immediately infused area, with no significant immune activation detected in cortical regions (data not shown).

Comparison of HA tag and hASM expression

We anticipated that an HA epitope tag might be required in order to distinguish expressed hASM from endogenous

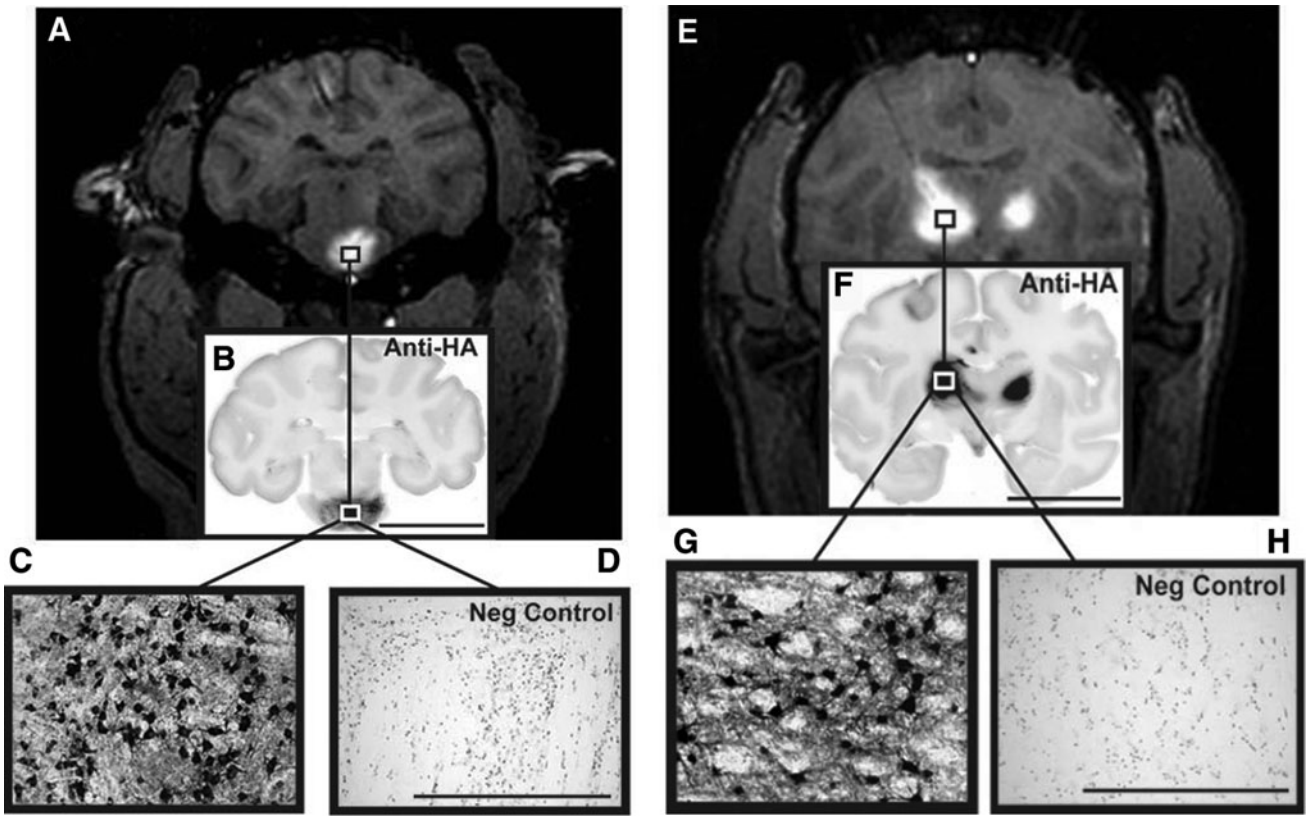

FIG. 4. AAV infusion and transduction in brainstem and thalamus. Shown are DICOM MR images representative of brainstem and thalamic infusion (**A** and **E**, respectively), and immunostained brain sections anatomically matched to the corresponding MR image (**B** and **F**). High-power magnification images demonstrate infusion epicenter with significant neuronal transduction (HA expression) in each targeted region (**C** and **D**), as compared with negative controls (**G** and **H**). Note that boxes drawn on the MR images are merely representative of the ROIs and are not to scale. Microscopic analysis was performed on NHP tissue perfused 5 weeks after AAV2-hASM-HA infusion. Scale bars: (**B** and **F**) 2 cm; (**C**, **D**, **G**, and **H**) 500 μm.

NHP ASM. However, we found that anti-HA and anti-hASM staining were superimposable with no evident staining of endogenous ASM (see Supplementary Fig. 7 at www.liebertonline.com/hum). This result confirmed that AAV2-hASM-HA can easily drive the expression of ASM to supraphysiological levels detected by immunostaining without the need for the HA tag.

Discussion

We have shown for the first time that AAV2 carrying the human ASM cDNA can be delivered safely into the NHP brainstem and thalamus with no apparent adverse effects. Moreover, we have demonstrated widespread distribution of gene expression throughout the large NHP brain with as

Table 1. Transgene Expression/Distribution in the Cerebral Cortex[a]

		NHP843		*NHP1210*		*NHP1260*		*NHP1228*	
Region	*Cortical area*	*L*	*R*	*L*	*R*	*L*	*R*	*L*	*R*
Prefrontal cortex	9/10/46	++	+++	—	++	++	+	+	—
Broca's area	44/45	+	+	+	++	+	+	++	+
Frontal eye field	8	+++	+++	+	+++	+++	++	+++	+
Secondary motor cortex	6	++	++	++	++	+++	++	+++	++
Anterior cingulate cortex	24/32	+	++	—	+	+	+	++	+
Somatosensory cortex	1/2/03	+++	++	++	+++	+++	+	+++	+
Primary motor cortex	4	++	++	++	+++	+++	++	+++	++
Posterior cingulate cortex	23/31	—	—	—	+	+	+	++	+

Abbreviations: L, left; NHP, nonhuman primate; R, right.
[a]Distribution of transduction: +++, ≥ 50 positive cells; ++, 10–49 positive cells; +, ≤9 positive cells; —, no transduced cells.

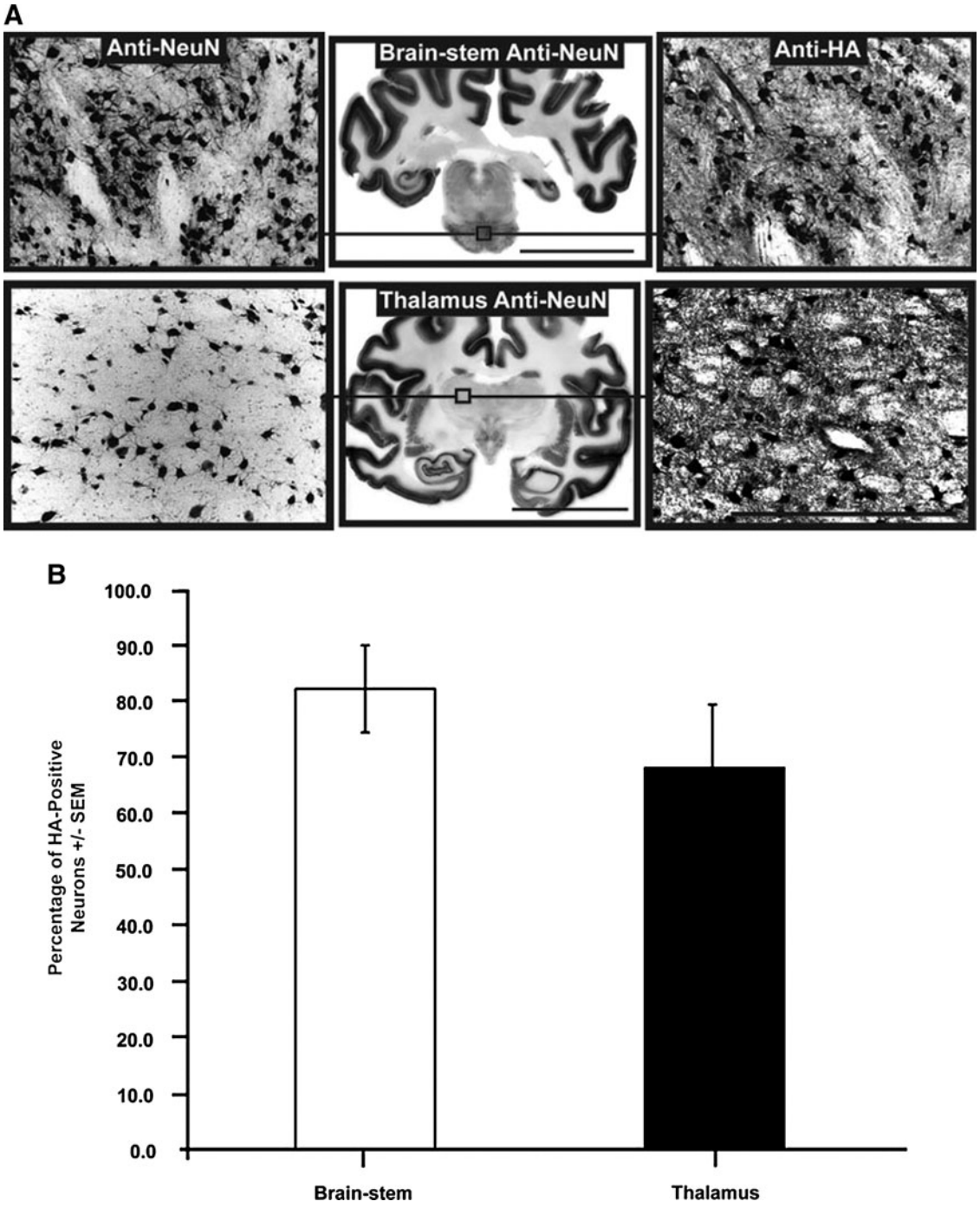

FIG. 5. High neuronal transduction numbers in targeted regions. (**A**) Cellular counting of randomized adjacent, histology-processed sections stained against neuronal marker (anti-NeuN) and HA tag epitope (anti-HA). (**B**) High neuronal transduction levels in the brainstem ($82 \pm 7.8\%$, $n = 4$) and in the thalamus ($68 \pm 11.3\%$, $n = 7$). No significant difference was found between levels of transduction efficiency in these two regions ($p > 0.05$). Microscopic analysis was performed on NHP tissue perfused 5 weeks after AAV2-hASM-HA infusion. Scale bars: for whole brain mounts, 2 cm; for immunostained sections, 500 μm.

few as three infusions via CED into brain regions clinically relevant to patients with NPD-A. In contrast, a gene therapy protocol for Canavan disease proposed that an AAV2 vector encoding aspartoacylase (ASPA) cDNA be injected into six sites bilaterally in the frontal, parietal, and occipital regions, delivering up to 150 μl/site (Janson *et al.*, 2002). Similarly, another protocol for AAV2-based gene therapy of late infantile neuronal ceroid lipofuscinosis (LINCL) proposed delivery into 12 target sites per brain (Crystal *et al.*, 2004). In our procedure, broad transgene expression in the brain seems to be possible with as few as three infusion sites, thereby reducing the invasiveness of the procedure

Table 2. Distribution Area (Gadoteridol) and Transgene Expression in Brainstem and Thalamus

Brainstem	*NHP*	*Gd (cm^2)*	*Histology (cm^2)*	*Percentage (%)*
	843	0.81	0.93	115
	1210	0.65	0.88	135
	1260	0.98	0.98	100
	1228	0.79	0.92	116
			Mean + SEM:	$117 \pm 7.2\%$
Thalamus	*NHP (L/R side)*	*Gd (cm^2)*	*Histology (cm^2)*	*Percentage (%)*
	843 (L)	0.82	0.88	107
	1210 (L)	0.21	0.20	94
	1260 (L)	0.39	0.28	71
	1228 (L)	0.41	0.19	45
	843 (R)	0.36	0.36	100
	1210 (R)	0.25	0.23	92
	1228 (R)	0.54	0.36	66
			Mean + SEM:	$82 \pm 8.4\%$

Abbreviations: Gd, gadoteridol; L, left; NHP, nonhuman primate; R, right.

and consequently reducing risk to these fragile pediatric patients.

RCD of AAV2-hASM-HA resulted in robust transduction in directly targeted regions with the therapeutic transgene, with 82% of neurons in the brainstem and 68% in the thalamus positive for HA. Expression was also found in areas distal to the infusion site. This is an important finding given that gene transport to distal locations in the CNS has been shown to have significant effects in the pathological correction of NPD in $ASM^{-/-}$ mice (Passini *et al.*, 2005) and has clinical implications for NPD-A.

The use of imaging to visualize cannula placement, as well as the distribution and monitoring of drug delivery, maximizes procedure efficacy and provides accurate targeting of the clinically relevant CNS anatomy (Fig. 1). RCD provides neurosurgeons with an added level of control and knowledge that the therapeutic agent has not been incorrectly delivered into a cerebrospinal fluid (CSF) compartment or undesired brain regions (Yin *et al.*, 2009). In addition, data showing significant reproducibility ($R^2 = 0.96$) of V_d:V_i ratios after repeated, targeted infusions into the same anatomical regions (Fig. 3) suggest that CED does not disturb the maintenance of normal tissue function and the movement of virions through the CNS parenchyma. This safety aspect is especially relevant for delivery into the immature nervous system of children with NPD-A.

Analysis of infusate delivery revealed a linear correlation between V_d and V_i ($R^2 = 0.93$) for CED procedures combining Gd only and AAV/Gd infusions (Fig. 2). This result accorded with findings from previous experiments describing the safety of CED with Gd-loaded liposomes (Krauze *et al.*, 2008), and is consistent with other observations from brainstem CED infusions in rodents, where linear increases in V_d proportional to increases in V_i were described (Sandberg *et al.*, 2002). We found volumetric dimensions of the brainstem to be extremely accommodating to delivery volumes up to 200 μl, with no apparent adverse effects. Fluctuation in this V_d:V_i linearity correlate with failure of infusate distribution as demonstrated previously by us in NHPs (Varenika *et al.*, 2008) and in a clinical brainstem infusion case, where nonlinearity was caused by leakage into the surrounding ventricular space (Lonser *et al.*, 2007). Along with infusate leakage (Varenika *et al.*, 2009), other factors such as infusion rate and cannula size have been shown to affect the efficacy of CED (Chen *et al.*, 1999). It should also be noted that V_d:V_i ratios are also affected by the composition of various anatomical regions, perhaps dependent on whether these regions are structurally composed of mainly gray or white matter (Szerlip *et al.*, 2007).

Targeted CED delivery to the brainstem and thalamus with the HA-tagged vector resulted in the global distribution of the human transgene. This result was verified by immunohistochemical techniques staining for either the HA tag epitope or the human transgene, demonstrating colocalized immunoreactivity and similar distribution patterns for both markers (Supplementary Fig. 7). The data resolved prior concerns, namely adequate detection and discrimination between the human transgene and endogenous monkey ASM. The fact that the HA tag did not engender a strong cell-mediated immune response is in line with previous observations that transduction of non-antigen-presenting cells such as neurons by AAV2 does not elicit a cell-mediated immune response, in contrast to vectors such as AAV1 that evince a broader tropism (Hadaczek *et al.*, 2009). The exact mechanism by which vector particles move within the CNS parenchyma has not been fully elucidated (Cearly and Wolfe, 2007). However, it is possible that transsynaptic transport might be contributing to the widespread distribution of AAV2-hASM-HA. In addition, previous observations from our laboratory have also speculated on alternative routes for gene trafficking, such as alongside axonal projections (Kells *et al.*, 2009) and through the perivascular space (Hadaczek *et al.*, 2006). It is also possible that highly interconnected projections of transfected neurons might secrete ASM to neighboring neurons, thus contributing to the spread of therapeutic agent to other regions not detectable by the immunohistochemical technique employed in this study. In agreement with this idea, correction of CNS pathology in ASM knockout mice occurred in distal regions where ASM expression was not detected (Passini *et al.*, 2005).

Targeting of brain regions containing numerous reciprocal connections such as the thalamus contributes greatly to the

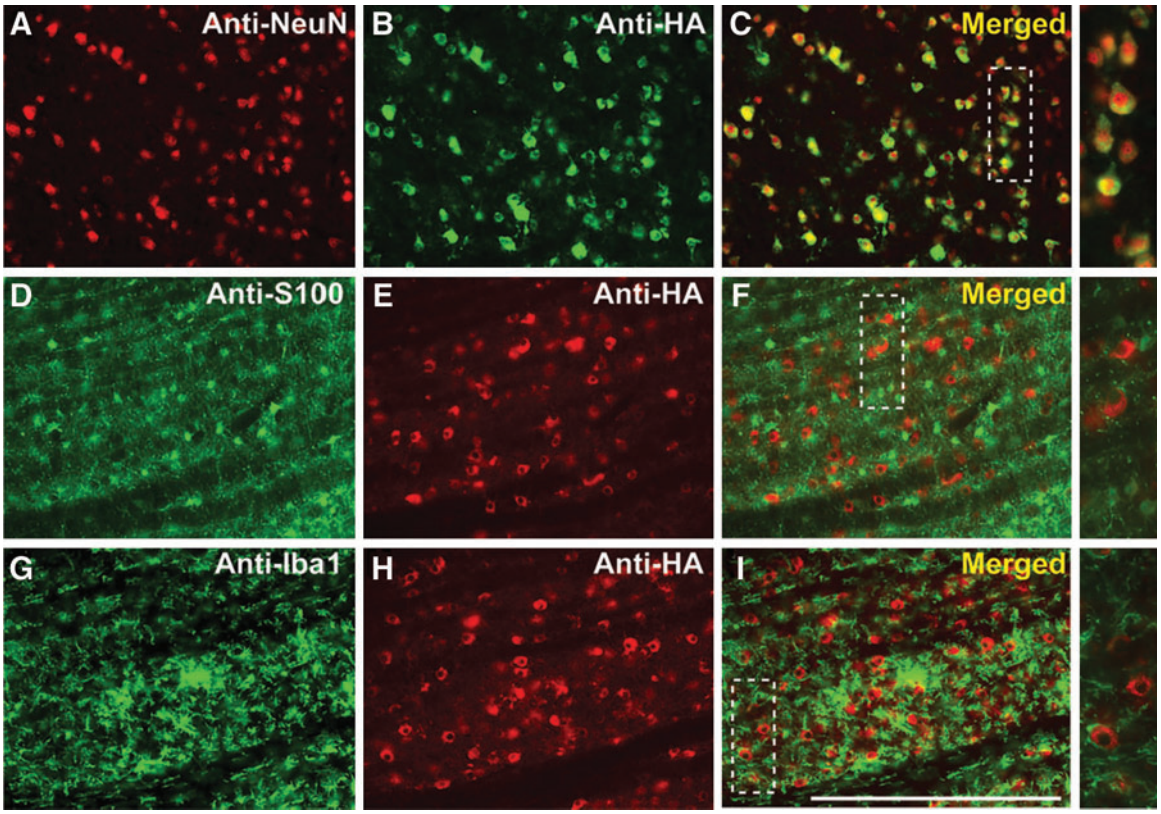

FIG. 6. Efficient neuronal transduction in brainstem. Immunostained brainstem sections indicate neuron-specific transduction (**A–C**) with no transduction observed in astrocytes (**D–F**) and/or microglia (**G–I**) (see high-magnification panels on the *right*). Note that the total number of colocalized NeuN/HA-positive cells was 61 of 63, representing 97% neuronal specificity. Scale bar: (**A–I**) 500 μm. Color images available online at www.liebertonline.com/hum.

distribution of therapeutic agents throughout the brain (Kells *et al.*, 2009). In fact, HA-positive neurons, indirectly indicative of AAV2 transduction, were found both in subcortical regions directly targeted by CED (Fig. 4) and in related cortical regions extending as far as the prefrontal cortex. Cortical distribution of this lysosomal enzyme was found in several clinically relevant areas such as the primary and secondary motor cortex, somatosensory cortex, and Broca's area (Table 1). We believe that the prominent gene transfer shown here sets the foundation for ASM gene replacement in the human CNS, an eminently achievable goal in that $ASM^{-/-}$ mice required only a slight increase of approximately 11–18% in enzyme activity to dramatically preserve normal CNS function (Marathe *et al.*, 2000).

RCD offers a high level of predictability in gene expression (Fig. 5; Table 2). We have reported similar findings with other transgenes delivered into NHP putamen (Fiandaca *et al.*, 2008b; Fiandaca *et al.*, 2009). In the brainstem, infusions of AAV2-hASM-HA resulted in a 17% greater area of transduction than was predicted by MRI. In contrast, thalamic infusions gave transduction areas equal to only 82% of that predicted by MRI. It is not clear why this is so, but previously we found that the V_d:V_i ratio of liposomes was greater in white matter than in regions of predominantly gray matter, such as putamen (Krauze *et al.*, 2005). It is also important to consider that transduction patterns with any type of parenchymal CNS delivery may vary when different AAV serotypes and transgenes are employed (Hadaczek *et al.*, 2009).

Clinically, AAV2 has been regarded as the vector of choice for CNS gene delivery for several reasons, including its relatively widespread use in neurological gene therapy in Parkinson's disease (Kaplitt *et al.*, 2007; Eberling *et al.*, 2008; Marks *et al.*, 2008; Christine *et al.*, 2009), its tropism for neurons (Bartlett *et al.*, 1998), and long-term CNS expression after delivery (Bankiewicz *et al.*, 2006; Daadi *et al.*, 2006). Consistent with previous observations, we have also demonstrated high efficiency and cellular tropism of AAV2 for neurons after CED, with no astrogliosis (Fig. 6) or systemic immune response within the CNS (data not shown). The use of AAV2 encoding human ASM has been described in several experiments, all of which have repeatedly reported the successful pathological correction of the pathology associated with low ASM activity in $ASM^{-/-}$ mice (Barbon *et al.*, 2005; Dodge *et al.*, 2005; Passini *et al.*, 2005, 2007).

We have safely delivered AAV2 particles to highly vascularized regions with no evidence of hemorrhage or significant tissue disruption. This study provides the foundation for translation of AAV2-hASM into clinical study, through the use of large animal models that facilitate the assessment of likely tropism, biodistribution, and persistence of gene therapy vectors in human clinical trials (Fiandaca *et al.*, 2008a). The fact that the movement of AAV is influenced by region-specific connectivity is an opportunity that needs to be explored further. The use of MRI-based CED of AAV2-hASM is a novel treatment approach that may

eventually provide significant neurological improvement to patients with NPD-A.

Acknowledgments

This study was supported by a grant to K.S.B. from NIH-NINDS (R01 NS056107-01).

Author Disclosure Statement

No competing financial interests exist.

References

Bankiewicz, K.S., Forsayeth, J., Eberling, J.L., Sanchez-Pernaute, R., Pivirotto, P., Bringas, J., Herscovitch, P., Carson, R.E., Eckelman, W., Reutter, B., and Cunningham, J. (2006). Long-term clinical improvement in MPTP-lesioned primates after gene therapy with AAVhAADC. Mol. Ther. 14, 564–570.

Barbon, C.M., Ziegler, R.J., Li, C., Armentano, D., Cherry, M., Desnick, R.J., Schuchman, E.H., and Cheng, S.H. (2005). AAV8-mediated hepatic expression of acid sphingomyelinase corrects the metabolic defect in the visceral organs of a mouse model of Niemann-Pick disease. Mol. Ther. 12, 431–440.

Barranger, J.M., and Novelli, E.A. (2001). Gene therapy for lysosomal storage disorders. Expert Opin. Biol. Ther. 1, 857–867.

Bartlett, J.S., Samulski, R.J., and McCown, T.J. (1998). Selective and rapid uptake of adeno-associated virus type 2 in brain. Hum. Gene Ther. 9, 1181–1186.

Barton, N.W., Brady, R.O., Dambrosia, J.M., Di Bisceglie, A.M., Doppelt, S.H., Hill, S.C., Mankin, H.J., Murray, G.J., Parker, R.I., Argoff, C.E., Grewal, R.P., and Yu, K.-T. (1991). Replacement therapy for inherited enzyme deficiency: Macrophage-targeted glucocerebrosidase for Gaucher's disease. N. Engl. J. Med. 324, 1464–1470.

Berger, A., Rosenthal, D., and Spiegel, S. (1995). Sphingosylphosphocholine, a signaling molecule which accumulates in Niemann-Pick disease type A, stimulates DNA-binding activity of the transcription activator protein AP-1. Proc. Natl. Acad. Sci. U.S.A. 92, 5885–5889.

Bosch, A., Perret, E., Desmaris, N., Trono, D., and Heard, J.M. (2000). Reversal of pathology in the entire brain of mucopolysaccharidosis type VII mice after lentivirus-mediated gene transfer. Hum. Gene Ther. 11, 1139–1150.

Cearly, C.C., and Wolfe, J.H. (2007). A single injection of an adeno-associated virus vector into nuclei with divergent connections results in widespread vector distribution in the brain and global correction of a neurogenetic disease. J. Neurosci. 27, 9928–9940.

Chen, M.Y., Lonser, R.R., Morrison, P.F., Governale, L.S., and Oldfield, E.H. (1999). Variables affecting convection-enhanced delivery to the striatum: A systematic examination of rate of infusion, cannula size, infusate concentration, and tissue-cannula sealing time. J. Neurosurg. 90, 315–320.

Christine, C.W., Starr, P.A., Larson, P.S., Eberling, J.L., Jagust, W.J., Hawkins, R.A., Vanbrocklin, H.F., Wright, J.F., Bankiewicz, K.S., and Aminoff, M.J. (2009). Safety and tolerability of putaminal AADC gene therapy for Parkinson's disease. Neurology 73, 1662–1669.

Crystal, R.G., Sondhi, D., Hackett, N.R., Kaminsky, S.M., Worgall, S., Stieg, P., Souweidane, M., Hosain, S., Heier, L., Ballon, D., Dinner, M., Wisniewski, K., Kaplitt, M., Greenwald, B.M., Howell, J.D., Strybing, K., Dyke, J., and Voss, H. (2004). Clinical protocol: Administration of a replication-deficient adeno-associated virus gene transfer vector expressing the human CLN2 cDNA to the brain of children with late infantile neuronal ceroid lipofuscinosis. Hum. Gene Ther. 15, 1131–1154.

Cunningham, J., Pivirotto, P., Bringas, J., Suzuki, B., Vijay, S., Sanftner, L., Kitamura, M., Chan, C., and Bankiewicz, K.S. (2008). Biodistribution of adeno-associated virus type-2 in nonhuman primates after convection-enhanced delivery to brain. Mol. Ther. 16, 1267–1275.

Daadi, M.M., Pivirotto, P., Bringas, J., Cunningham, J., Forsayeth, J., Eberling, J., and Bankiewicz, K.S. (2006). Distribution of AAV2-hAADC24 transduced cells after 3 years in Parkinsonian monkeys. Neuroreport 17, 201– 204.

Dodge, J.C., Clarke, J., Song, A., Bu, J., Yang, W., Taksir, T.V., Griffiths, D., Zhao, M.A., Schuchman, E.H., Cheng, S.H., O'Riordan, C.R., Shihabuddin, L.S., Passini, M.A., and Stewart, G.R. (2005). Gene transfer of human acid sphingomyelinase corrects neuropathology and motor deficits in a mouse model of Niemann-Pick type A disease. Proc. Natl. Acad. Sci. U.S.A. 102, 17822–17827.

Eberling, J.L., Jagust, W.J., Christine, C.W., Starr, P., Larson, P., Bankiewicz, K.S., and Aminoff, M.J. (2008). Results from a phase I safety trial of hAADC gene therapy for Parkinson disease. Neurology 70, 1980–1983.

Fiandaca, M., Forsayeth, J., and Bankiewicz, K. (2008a). Current status of gene therapy trials for Parkinson's disease. Exp. Neurol. 209, 51–57.

Fiandaca, M.S., Forsayeth, J.R., Dickinson, P.J., and Bankiewicz, K.S. (2008b). Image-guided convection-enhanced delivery platform in the treatment of neurological diseases. Neurotherapeutics 5, 123–127.

Fiandaca, M.S., Varenika, V., Eberling, J., McKnight, T., Bringas, J., Pivirotto, P., Beyer, J., Hadaczek, P., Bowers, W., Park, J., Federoff, H., Forsayeth, J., and Bankiewicz, K.S. (2009). Real-time MR imaging of adeno-associated viral vector delivery to the primate brain. Neuroimage 47(Suppl. 2), T27–T35.

Graber, D., Salvayre, R., and Levade, T. (1994). Accurate differentiation of neuronopathic and nonneuronopathic forms of Niemann-Pick disease by evaluation of the effective residual lysosomal sphingomyelinase activity in intact cells. J. Neurochem. 63, 1060–1068.

Hadaczek, P., Yamashita, Y., Mirek, H., Tamas, L., Bohn, C.M., Noble, C., Park, J.W., and Bankiewicz, K.S. (2006). The "perivascular pump" driven by arterial pulsation is a powerful mechanism for the distribution of therapeutic molecules within the brain. Mol. Ther. 14, 69–78.

Hadaczek, P., Forsayeth, J., Mirek, H., Munson, K., Bringas, J., Pivirotto, P., McBride, J.L., Davidson, B.L., and Bankiewicz, K.S. (2009). Transduction of nonhuman primate brain with adeno-associated virus serotype 1: Vector trafficking and immune response. Hum. Gene Ther. 20, 225–237.

Hsich, G., Sena-Esteves, M., and Breakefield, X.O. (2002). Critical issues in gene therapy for neurologic disease. Hum. Gene Ther. 13, 579–604.

Janson, C., McPhee, S., Bilaniuk, L., Haselgrove, J., Testaiuti, M., Freese, A., Wang, D.J., Shera, D., Hurh, P., Rupin, J., Saslow, E., Goldfarb, O., Goldberg, M., Larijani, G., Sharrar, W., Liouterman, L., Camp, A., Kolodny, E., Samulski, J., and Leone, P. (2002). Clinical protocol. Gene therapy of Canavan disease: AAV-2 vector for neurosurgical delivery of aspartoacylase gene (ASPA) to the human brain. Hum. Gene Ther. 13, 1391–1412.

Kaplitt, M.G., Feigin, A., Tang, C., Fitzsimons, H.L., Mattis, P., Lawlor, P.A., Bland, R.J., Young, D., Strybing, K., Eidelberg, D., and During, M.J. (2007). Safety and tolerability of gene

therapy with an adeno-associated virus (AAV) borne GAD gene for Parkinson's disease: An open label, phase I trial. Lancet 369, 2097–2105.

Kells, A.P., Hadaczek, P., Yin, D., Bringas, J., Varenika, V., Forsayeth, J., and Bankiewicz, K.S. (2009). Efficient gene therapy-based method for the delivery of therapeutics to primate cortex. Proc. Natl. Acad. Sci. U.S.A. 106, 2407–2411.

Kim, E.Y., Hong, Y.B., Lai, Z., Kim, H.J., Cho, Y.H., Brady, R.O., and Jung, S.C. (2004). Expression and secretion of human glucocerebrosidase mediated by recombinant lentivirus vectors *in vitro* and *in vivo*: Implications for gene therapy of Gaucher disease. Biochem. Biophys. Res. Commun. 318, 381–390.

Krauze, M.T., McKnight, T.R., Yamashita, Y., Bringas, J., Noble, C.O., Saito, R., Geletneky, K., Forsayeth, J., Berger, M.S., Jackson, P., Park, J.W., and Bankiewicz, K.S. (2005). Real-time visualization and characterization of liposomal delivery into the monkey brain by magnetic resonance imaging. Brain Res. Brain Res. Protoc. 16, 20–26.

Krauze, M.T., Vandenberg, S.R., Yamashita, Y., Saito, R., Forsayeth, J., Noble, C., Park, J., and Bankiewicz, K.S. (2008). Safety of real-time convection-enhanced delivery of liposomes to primate brain: A long-term retrospective. Exp. Neurol. 210, 638–644.

Lonser, R.R., Warren, K.E., Butman, J.A., Quezado, Z., Robison, R.A., Walbridge, S., Schiffman, R., Merrill, M., Walker, M.L., Park, D.M., Croteau, D., Brady, R.O., and Oldfield, E.H. (2007). Real-time image guided direct convective perfusion of intrinsic brainstem lesions: Technical note. J. Neurosurg. 107, 190–197.

Marathe, S., Miranda, S.R., Devlin, C., Johns, A., Kuriakose, G., Williams, K.J., Schuchman, E.H., and Tabas, I. (2000). Creation of a mouse model for non-neurological (type B) Niemann-Pick disease by stable, low level expression of lysosomal sphingomyelinase in the absence of secretory sphingomyelinase: Relationship between brain intra-lysosomal enzyme activity and central nervous system function. Hum. Mol. Genet. 9, 1967–1976.

Marks, W.J., Jr., Ostrem, J.L., Verhagen, L., Starr, P.A., Larson, P.S., Bakay, R.A., Taylor, R., Cahn-Weiner, D.A., Stoessl, A.J., Olanow, C.W., and Bartus, R.T. (2008). Safety and tolerability of intraputaminal delivery of CERE-120 (adeno-associated virus serotype 2-neurturin) to patients with idiopathic Parkinson's disease: An open-label, phase I trial. Lancet Neurol. 7, 400–408.

Matsushita, T., Elliger, S., Elliger, C., Podsakoff, G., Villarreal, L., Kurtzman, G.J., Iwaki, Y., and Colosi, P. (1998). Adeno-associated virus vectors can be efficiently produced without helper virus. Gene Ther. 5, 938–945.

Otterbach, B., and Stoffel, W. (1995). Acid sphingomyelinase-deficient mice mimic the neurovisceral form of human lysosomal storage disease (Niemann-Pick disease). Cell 81, 1053–1061.

Passini, M.A., Macauley, S.L., Huff, M.R., Taksir, T.V., Bu, J., Wu, I.H., Piepenhagen, P.A., Dodge, J.C., Shihabuddin, L.S., O'Riordan, C.R., Schuchman, E.H., and Stewart, G.R. (2005). AAV vector-mediated correction of brain pathology in a mouse model of Niemann-Pick A disease. Mol. Ther. 11, 754–762.

Passini, M.A., Bu, J., Fidler, J.A., Ziegler, R.J., Foley, J.W., Dodge, J.C., Yang, W.W., Clarke, J., Taksir, T.V., Griffiths, D.A., Zhao, M.A., O'Riordan, C.R., Schuchman, E.H., Shihabuddin, L.S., and Cheng, S.H. (2007). Combination brain and systemic injections of AAV provide maximal functional and survival benefits in the Niemann-Pick mouse. Proc. Natl. Acad. Sci. U.S.A. 104, 9505–9510.

Peltola, M., Kyttala, A., Heinonen, O., Rapola, J., Paunio, T., Revah, F., Peltonen, L., and Jalanko, A. (1998). Adenovirus-mediated gene transfer results in decreased lysosomal storage in brain and total correction in liver of aspartylglucosaminuria (AGU) mouse. Gene Ther. 5, 1314–1321.

Sandberg, D.I., Edgar, M.A., and Souweidane, M.M. (2002). Effect of hyperosmolar mannitol on convection-enhanced delivery into the rat brain stem. J. Neurooncol. 58, 187–192.

Szerlip, N.J., Walbridge, S., Yang, L., Morrison, P.F., Degen, J.W., Jarrell, S.T., Kouri, J., Kerr, P.B., Kotin, R., Oldfield, E.H., and Lonser, R.R. (2007). Real-time imaging of convection-enhanced delivery of viruses and virus-sized particles. J. Neurosurg. 107, 560–567.

Varenika, V., Dickenson, P., Bringas, J., Lecouteur, R., Higgins, R., Park, J.W., Fiandaca, M., Berger, M.S., Sampson, J.H., and Bankiewicz, K.S. (2008). Real-time imaging of CED in the brain permits detection of infusate leakage. J. Neurosurg. 109, 874–880.

Varenika, V., Kells, A.P., Valles, F., Hadaczek, P., Forsayeth, J., and Bankiewicz, K.S. (2009). Controlled dissemination of AAV vectors in the primate brain. Prog. Brain Res. 175, 163–172.

Watson, D.J., and Wolfe, J.H. (2003). Lentiviral vectors for gene transfer to the central nervous system: Applications in lysosomal storage disease animal models. Methods Mol. Med. 76, 383–403.

Wright, J.F., Qu, G., Tang, C., and Sommer, J.M. (2003). Recombinant adenoassociated virus: Formulation challenges and strategies for a gene therapy vector. Curr. Opin. Drug Discov. Dev. 6, 174–178.

Yin, D., Valles, F.E., Fiandaca, M.S., Bringas, J., Gimenez, F., Berger, M.S., Forsayeth, J., and Bankiewicz, K.S. (2009). Optimal region of the putamen for image-guided convection-enhanced delivery of therapeutics in human and non-human primates. Neuroimage (in press).

Yin, D., Richardson, R.M., Fiandaca, M.S., Bringas, J., Forsayeth, J., Berger, M.S., and Bankiewicz, K.S. (2010). Cannula placement for effective convection-enhanced delivery in the non-human primate thalamus and brainstem: Implications for clinical delivery of therapeutics. J. Neurosurg. (in press).

Ziegler, R.J., Yew, N.S., Li, C., Cherry, M., Berthelette, P., Romanczuk, H., Ioannou, Y.A., Zeidner, K.M., Desnick, R.J., and Cheng, S.H. (1999). Correction of enzymatic and lysosomal storage defects in Fabry mice by adenovirus-mediated gene transfer. Hum. Gene Ther. 10, 1667–1682.

Address correspondence to:
Dr. Krystof S. Bankiewicz
Department of Neurosurgery
University of California San Francisco
1855 Folsom Street, MCB, Room 226
San Francisco, CA 94103

E-mail: Krystof.Bankiewicz@ucsf.edu

Received for publication March 9, 2010;
accepted after revision April 20, 2010.

Published online: July 21, 2010.